FULL PAPER

Dalton
www.rsc.org/dalton

The interplay between steric repulsions and metal–metal bonding in $[Ru_2(\mu\text{-}Cl)_3(PR_3)_6]^{z+}$, R = H, Me, Et, z = 1, 2, 3: a hybrid QM/MM study †

Sushilla Z. Knottenbelt,[a] John E. McGrady *[a] and Graham A. Heath[b]

[a] *Department of Chemistry, The University of York, Heslington, York, UK YO10 5DD. E-mail: jem15@york.ac.uk*

[b] *The Research School of Chemistry, The Australian National University, Canberra, ACT 0200, Australia*

Received 2nd September 2002, Accepted 18th November 2002
First published as an Advance Article on the web 12th December 2002

The hybrid quantum/molecular mechanics methodology is used to examine the interplay between metal–metal bonding and steric effects in a series of isostructural redox-related ruthenium dimers. Potential energy surfaces for the various electronic states arising from (d^6d^6) (1+), (d^5d^6) (2+) and (d^5d^5) (3+) configurations are explored. Somewhat counterintuitively, the bulky groups on the phosphine ligands are found to have most effect when the Ru–Ru bonding is *strongest*. The origin of this trend has been traced to the nature of the steric interactions, which are largely between the bridging halides and the substituents on the phosphine. As the Ru–Ru bond contracts, a concertina-like motion displaces the halides away from the trigonal axis and towards the phosphine substituents. The resulting competition between Ru–Ru bonding and steric repulsions means that varying the bulk of the phosphine provides an efficient mechanism for tuning or even completely eliminating the metal–metal bond.

Introduction

The emergence of density functional theory over the past ten years has revolutionised the way in which the electronic structure of transition metal systems is treated. Most significantly, the realistic treatment of the total energy within DFT affords accurate equilibrium structures and reaction pathways. The size of the system amenable to calculation is, in principle, limited only by the computational resources available, and the rapid development of hardware during the same period means that rather large systems containing several metal ions can now be tackled.[1] The effective treatment of substituents on ligands, however, remains a considerable problem, due to the large number of such groups typically present in a molecule, and also to their high degree of conformational flexibility. As a result, it has been common practice to reduce ligands to their simplest model forms, a typical example being the replacement of any phosphine, PR_3, with the parent PH_3. Whilst this procedure is computationally expedient, it is clear that any of the subtle (and often not so subtle) changes in chemistry associated with a change in phosphine will be beyond the scope of the computational experiment. Very recently, hybrid quantum mechanics/molecular mechanics (QM/MM) techniques[2] have emerged as a viable means of addressing this problem. The basis of the technique lies in retaining an accurate quantum mechanical description of the core of the molecule (typically the metal centres and first coordination sphere), while treating the peripheral substituents (the R groups in the above example) with less expensive molecular mechanics-based protocols. It is important to emphasise that only the steric influence of the substituents is incorporated in this way – inductive effects are not transmitted across the boundary between the QM and MM regions. Nevertheless, hybrid QM/MM has proved to be a powerful technique, particularly in cases where the steric influence of the substituents is of similar magnitude, in energetic terms, to important electronic interactions within the core. In such circumstances, the incorporation of the full ligand can cause dramatic changes in structure and properties.[3]

In recent years, we have been interested in describing the interactions between transition metal ions in clusters, with a particular emphasis on systems that lie on or near the borderline between weak magnetic coupling and strong covalent bonding.[4,5] In certain cases, it is possible to isolate a single molecule in two distinct forms, differing only in the nature of the interaction between the metal ions.[5b,6] More generally, however, it is likely that such borderline examples will have very flat potential energy surfaces, and hence structures that depend strongly on the environment of the molecule. The $[Mo_2Cl_9]^{3-}$ anion is just such an example, where the potential energy surface is very flat in the region 2.5 Å < Mo–Mo < 2.9 Å, despite the fact that the δ_π components of the Mo–Mo triple bond are effectively eliminated at larger separations.[4b] It is not surprising, in such circumstances, that the size of the cation, A, in $A_3Mo_2Cl_9$ salts has a substantial effect on the Mo–Mo bond length as well as the magnetic properties of the anion.[7] These solid-state studies illustrate the impact of *inter*molecular forces on the nature of the metal–metal bond, but it is possible that *intra*molecular forces may play a similar role. In this paper, we explore this possibility by examining the influence of phosphine ligand on the electronic structure and geometry of a series of bimetallic systems, $[Ru_2(\mu\text{-}Cl)_3(PR_3)_6]^{z+}$. The qualitative features of the bonding in these face-shared bioctahedral systems are well established (Scheme 1).[4,8] The t_{2g}-based orbitals of the parent

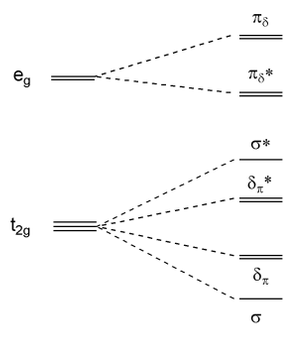

Scheme 1 Schematic MO diagram for a face-sharing bioctahedron.

† Electronic supplementary information (ESI) available: rotatable 3-D diagrams in CHIME format. See http://www.rsc.org/suppdata/dt/b2/b208530e/

DOI: 10.1039/b208530e

Table 1 Crystallographic data for $[Ru_2(\mu\text{-}Cl)_3(PR_3)_6]^+$ cations

	Ru–Ru/Å	Ru–Cl/Å	Ru–P/Å	Ref.
$[Ru_2(\mu\text{-}Cl)_3(PMe_3)_6]^+$	3.37	2.50	2.26	8*a*, 13
	3.27	2.48	2.25	8*b*
$[Ru_2(\mu\text{-}Cl)_3(PMe_2Ph)_6]^+$	3.39	2.49	2.29	9
$[Ru_2(\mu\text{-}Cl)_3(PEt_2Ph)_6]^+$	3.44	2.48	2.32	10
$[Ru_2(\mu\text{-}Cl)_3(PBu_3)_6]^+$	3.39	2.49	2.30	11
$[Ru_2(\mu\text{-}Cl)_3(MeC(CH_2PPh_2)_3)_2]^+$	3.46	2.49	2.31	12

octahedra combine to form bonding and antibonding combinations with local σ and δ_π symmetry, while the orbitals derived from the octahedral e_g set have local π_δ symmetry. The phosphine capped systems are isolated as the monocations, where the closed shell configuration (d^6) of the Ru^{II} ions precludes any net bonding interaction, leading to rather large Ru–Ru separations (3.2–3.5 Å, see Table 1).[8–12] In a series of detailed spectroelectrochemical experiments, Heath and co-workers have reversibly oxidised these complexes,[13] first to $[Ru_2(\mu\text{-}Cl)_3(PR_3)_6]^{2+}$ and then to $[Ru_2(\mu\text{-}Cl)_3(PR_3)_6]^{3+}$. Successive oxidation generates vacancies in the t_{2g} subshell, and can give rise, at least in principle, to a Ru–Ru hemibond ($z = 2$) and ultimately to a full covalent single bond where $z = 3$. Whilst no crystallographic data are available for either of the oxidised forms, the structures of the isoelectronic species $[Ru_2(\mu\text{-}Cl)_3(NH_3)_6]^{2+}$ (d^6d^5)[14] and $[Ru_2(\mu\text{-}Cl)_3Cl_6]^{3-}$ (d^5d^5),[15] are known, with Ru–Ru separations of 2.753(4) Å and 2.725(3) Å, respectively. Spectroscopic results suggest that $[Ru_2(\mu\text{-}Cl)_3(PMe_3)_6]^{2+}$ is rather similar to the ammine-capped analogue (ruthenium 'blue'),[13] with a characteristic intense band in the visible region assigned to the σ⟶σ* transition (Scheme 1). However, the σ⟶σ* band appears at significantly lower energy in the phosphine-capped species and is further red-shifted when PMe_3 is replaced by PEt_3, suggesting that the bulkier phosphine weakens the Ru–Ru bond. In separate contributions, Yeomans *et al.*[13] and Clucas *et al.*[16] have debated the nature of the bonding in these complexes, and independently concluded that steric interactions between the $Ru(\mu\text{-}Cl)_3Ru$ core and the terminal ligands may be responsible for this destabilisation of the Ru–Ru bond (Scheme 2). In this

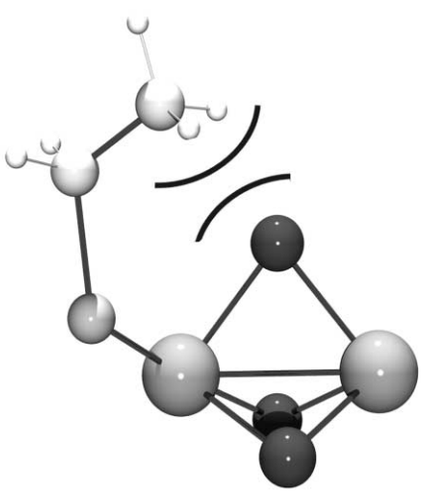

Scheme 2 Steric repulsions between bridging halides and the terminal ligands.

paper, we employ the hybrid QM/MM method to explore this proposal in the context of the series $[Ru_2(\mu\text{-}Cl)_3(PR_3)_6]^{1+/2+/3+}$. As noted above, the influence of the substituents on the phosphine will clearly be most dramatic when steric interactions are of similar magnitude to electronic interactions within the core. Given that successive oxidation causes an increase in Ru–Ru bond order from 0 to 0.5 to 1, it is likely that the substituents will have a very different influence on structure in the different oxidation states.

Computational details

All calculations described in this paper were performed using the Amsterdam Density Functional (ADF) program, ADF2000.02,[17] developed by Baerends and co-workers. A double-ζ Slater-type basis set, extended with a single polarisation function, was used to describe the hydrogen, nitrogen, phosphorus and chlorine atoms, while ruthenium was modeled with a triple-ζ basis set. Electrons in orbitals up to and including 1s {N}, 2p{P, Cl} and 4p{Ru} were considered part of the core and treated in accordance with the frozen core approximation. The local density approximation (LDA) was employed in all cases,[18] along with the local exchange-correlation potential of Vosko, Wilk and Nusair.[19] Where gradient corrections to exchange and correlation were employed, they were those proposed by Becke[20] and Perdew (BP86).[21] All structures were optimised using the gradient algorithm of Versluis and Ziegler.[22] In the hybrid quantum mechanics/molecular mechanics calculations, the $[Ru_2(\mu\text{-}Cl)_3(PH_3)_6]^{z+}$ core was treated using DFT as described above, while the molecular mechanics partition included the alkyl or aryl groups on the phosphines. Parameters were taken from the Sybyl force field,[23] with the exception of van der Waals parameters for Ru, which were taken from the UFF force field.[24] Potential energy curves were generated by fixing the Ru–Ru distance and allowing all other parameters to vary within the constraints of the appropriate point group.

Results and discussion

Optimised structures of $[Ru_2(\mu\text{-}Cl)_3Cl_6]^{3-}$, $[Ru_2(\mu\text{-}Cl)_3(NH_3)_6]^{2+}$: calibration of theory with experiment

The electronic structure of face-shared bioctahedra such as $[Ru_2(\mu\text{-}Cl)_3Cl_6]^{3-}$ and $[Ru_2(\mu\text{-}Cl)_3(NH_3)_6]^{2+}$ is well documented,[4,8] and is not the primary focus of this paper. Nevertheless, these two complexes provide an opportunity to assess the ability of a pure QM calculation to accurately model structural properties, particularly the Ru–Ru separation, in the absence of complicating steric factors. Optimised structural parameters (LDA and BP86) for both complexes are summarised in Table 2, along with the available crystallographic data. The calculated Ru–Ru separation is longer in the NH_3-capped species, consistent with the decrease in Ru–Ru bond order from 1.0 to 0.5, and the agreement between experiment and theory, at least at the LDA level, is striking. Optimised Ru–Ru bond lengths are within 0.04 Å of experiment, while the error in metal–ligand bonds (terminal and bridging) is not more than 0.03 Å in any case. The inclusion of gradient corrections in the model Hamiltonian results in a significantly poorer agreement, both in terms of metal–metal and metal–ligand distance. The relatively poor performance of gradient corrections in describing metal–metal bonds has been noted previously.[4c]

Optimised structures of $[Ru_2(\mu\text{-}Cl)_3(PR_3)_6]^+$, R = H, Me and Et: evaluation of the hybrid QM/MM methodology

In this section, we assess the steric influence of substituents on the phosphine ligands (incorporated through the hybrid QM/MM methodology) on the structure of the inner {Ru-

Table 2 Comparison of computed and crystallographic data for $[Ru_2(\mu\text{-}Cl)_3(NH_3)_6]^{2+}$ and $[Ru_2(\mu\text{-}Cl)_3Cl_6]^{3-}$

		Ru–Ru/Å	Ru–μ-Cl/Å	Ru–Cl_t/N/Å	Ref.
$[Ru_2(\mu\text{-}Cl)_3(NH_3)_6]^{2+}$	Expt.	2.753(4)	2.395	2.111	14
	LDA	2.79	2.43	2.11	
	BP86	2.91	2.48	2.17	
$[Ru_2(\mu\text{-}Cl)_3Cl_6]^{3-}$	Expt.	2.725(3)	2.391	2.332	15
	LDA	2.75	2.41	2.39	
	BP86	2.88	2.48	2.46	

Table 3 QM/MM optimised structural parameters for $[Ru_2(\mu\text{-}Cl)_3(PR_3)_6]^+$

	Ru–Ru/Å	Ru–Cl/Å	Ru–P/Å
$[Ru_2(\mu\text{-}Cl)_3(PH_3)_6]^+$	3.17	2.48	2.26
$[Ru_2(\mu\text{-}Cl)_3(PMe_3)_6]^+$	3.21	2.48	2.27
$[Ru_2(\mu\text{-}Cl)_3(PEt_3)_6]^+$	3.33	2.44	2.33

$(\mu\text{-}Cl)_3Ru\}$ core. The discussion at this stage is restricted to the monocations, for which structural data are available, and where the (d^6d^6) electronic configuration precludes direct Ru–Ru bonding. These closed-shell systems allow us to assess the steric influence of the ligands in isolation, thus providing a benchmark for subsequent studies of the oxidised species, where the steric factors are in direct competition with metal–metal bonding. Optimised structures of $[Ru_2(\mu\text{-}Cl)_3(PH_3)_6]^+$, $[Ru_2(\mu\text{-}Cl)_3(PMe_3)_6]^+$ and $[Ru_2(\mu\text{-}Cl)_3(PEt_3)_6]^+$ are summarised in Table 3.

The optimised Ru–Ru separation is, for all phosphines, considerably longer than in either $[Ru_2(\mu\text{-}Cl)_3Cl_6]^{3-}$or $[Ru_2(\mu\text{-}Cl)_3(NH_3)_6]^{2+}$, consistent with the absence of any net bond. However, the value of 3.17 Å for the simplest model phosphine, PH_3, is shorter than the shortest distance observed in any of the crystallographically characterised complexes, suggesting that the substituents do play a significant role in determining the structure of the $\{Ru(\mu\text{-}Cl)_3Ru\}$ core. Replacing the terminal hydrogen atoms with methyl groups presents an immediate problem, in that the number of possible conformations of the 18 methyl groups is extremely large, and identifying the global minimum is far from trivial. In such circumstances, it is common practice to be guided by crystallographic data, and our initial starting orientation, illustrated in Scheme 3, is taken from

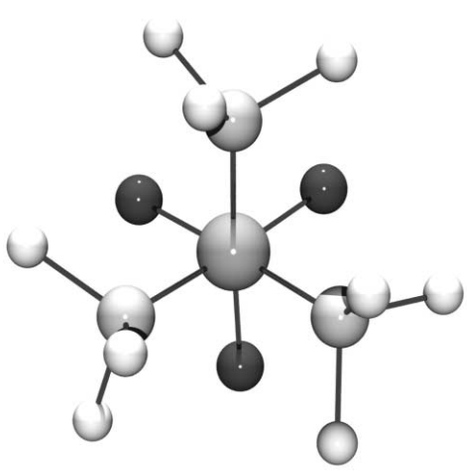

Scheme 3 Orientation of the Me groups in the crystal structure of $[Ru_2(\mu\text{-}Cl)_3(PMe_3)_6]^+$.

the crystal structure described by Heath *et al.*[8a,13] In the optimised structure, the Ru–Ru separation of 3.21 Å is 0.04 Å longer than in the PH_3-capped species, and more consistent with the values observed in the crystal structures. The incorporation of the methyl groups in their crystallographic orientation poses one further problem, in that all symmetry elements are eliminated. In addition to the significantly greater computational effort associated with calculations performed without symmetry, it is no longer possible to distinguish orbitals of σ and δ_π symmetry, a process that will prove invaluable to the interpretation of the electronic structure. It would clearly be favourable to symmetrise the methyl groups in such a way that the D_{3h} point symmetry of the $Ru_2(\mu\text{-}Cl)_3$ core is restored, a process that can be achieved by imposing a rotation of approximately 40° about each Ru–P bond. This symmetrisation causes a 50 kJ mol^{-1} increase in the total energy but, significantly, there is little change in the optimised structure of the $\{Ru(\mu\text{-}Cl)_3Ru\}$ core. In fact, potential energy curves (Fig. 1) for

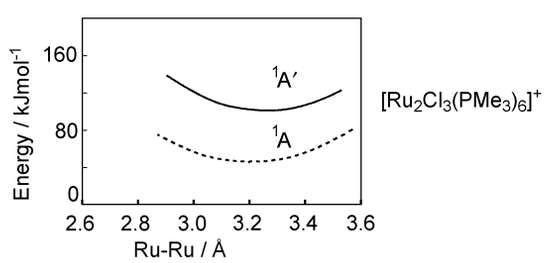

Fig. 1 Potential energy curves for non-symmetrised (^1A) and symmetrised ($^1A_1'$) states of $[Ru_2(\mu\text{-}Cl)_3(PMe_3)_6]^+$. The zero of energy is arbitrary.

the Ru–Ru stretch for symmetrised ($^1A_1'$) and non-symmetrised (^1A) orientations of the Me groups in $[Ru_2(\mu\text{-}Cl)_3(PMe_3)_6]^+$ are almost identical, other than a uniform upward shift of ~50 kJ mol^{-1} (the absolute zero of energy in Fig. 1 is arbitrary). Moreover, the decomposition of the total energy into separate components for the QM and MM regions indicates that the 50 kJ mol^{-1} destabilisation of the symmetrised structure is contained almost entirely within the MM partition, while the energy of the QM region changes by less than 5 kJ mol^{-1}. Thus both energetic and structural criteria suggest that symmetrisation does not significantly perturb the halide-bridged diruthenium core. In the context of this study this is an important observation, as it suggests that symmetrisation of the terminal ligands, with its attendant advantages, both in terms of cost and the control over the electronic state, does not significantly affect our conclusions regarding the nature of the interaction between the metal ions.

The PEt_3 ligands present a further degree of complexity, as the number of possible conformers is increased dramatically by the increase in length of the alkyl chain. Crystallographic data, in this case taken from the known structure of $[Os_2(\mu\text{-}Cl)_3(PEt_3)_6]^+$,[25] again provide a logical starting point (Scheme 4). The influence of the ethyl substituents on the bimetallic unit is much more dramatic, and the Ru–Ru separation increases to 3.33 Å. Whilst there are no structural data available for $[Ru_2(\mu\text{-}Cl)_3(PEt_3)_6]^+$, it is clear that this increase is consistent with the experimental trend towards longer separations for bulkier substituents (Table 1). Analysis of the optimised structure clearly reveals the origin of this trend: the shortest non-bonded contacts between the ethyl groups and the halide bridges are only 2.62 Å, significantly shorter than the corresponding values of 2.88 Å in the methyl-substituted system.

Table 4 QM/MM optimised structural parameters for symmetrised states of $[Ru_2(\mu\text{-}Cl)_3(PR_3)_6]^{2+}$

		Ru–Ru/Å	E_{rel}/kJ mol^{-1}
$[Ru_2(\mu\text{-}Cl)_3(PH_3)_6]^{2+}$	$^2A_2''$	2.90	0
	$^2E''$	3.17	35
$[Ru_2(\mu\text{-}Cl)_3(PMe_3)_6]^{2+}$	$^2A_2''$	3.05	0
	$^2E''$	3.26	17
$[Ru_2(\mu\text{-}Cl)_3(PEt_3)_6]^{2+}$	$^2A_2''$	3.12	0
	$^2E''$	3.33	2

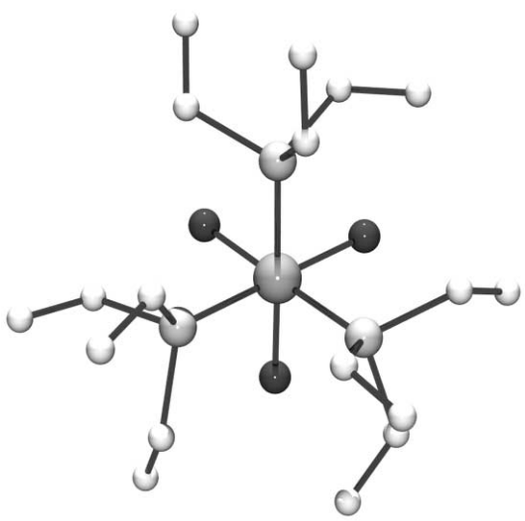

Scheme 4 Orientation of the Et groups in the crystal structure of $[Os_2(\mu\text{-}Cl)_3(PEt_3)_6]^+$.

Thus these preliminary results seem to confirm the picture suggested by Heath and Armstrong [13,16] illustrated in Scheme 2, where steric repulsions between the halide bridges and the remote substituents are responsible for the elongation of the Ru–Ru distance. Symmetrisation of the $(PEt_3)_3$ array to recover D_{3h} symmetry again destabilises the system, this time by some 150 kJ mol^{-1}, consistent with the greater congestion compared to the PMe_3 analogue, but again does not dramatically alter the optimised Ru–Ru separation. The partitioning of energy into QM and MM regions also confirms that the destabilisation is not associated with significant changes in the QM core, and must therefore be caused largely by unfavourable interactions *between* the ethyl groups. Thus, just as for the PMe_3 ligands, the orientation of the substituents on the phosphine, although critical in terms of absolute energies, does not play a significant role in determining the properties of the $Ru_2(\mu\text{-}Cl)_3$ core.

Structure and bonding in $[Ru_2(\mu\text{-}Cl)_3(PR_3)_6]^{2+}$

As noted in the introductory section, one-electron oxidation generates a vacancy in the t_{2g} manifold, and therefore opens up the possibility of metal–metal bonding. In these circumstances, the sterically induced elongation of the Ru–Ru separation discussed in the previous section will act in direct opposition to Ru–Ru bonding, which necessarily causes a contraction. Potential energy curves (calculated in a D_{3h}-symmetric structure) for the parent PH_3-capped structure, $[Ru_2(\mu\text{-}Cl)_3(PH_3)_6]^{2+}$, are shown in Fig. 2a, and optimised Ru–Ru separations and relative energies are collected in Table 4. The two curves correspond to removal of an electron from an orbital of a_2'' (σ) or e'' (δ_π) symmetry, generating states of $^2A_2''$ and $^2E''$ symmetry, respectively. The global minimum is clearly the former, with a relatively short Ru–Ru bond length of 2.90 Å, rather similar to the distance observed in the ammine-capped analogue, $[Ru_2(\mu\text{-}Cl)_3(NH_3)_6]^{2+}$. In the $^2E''$ state, the singly occupied orbital has δ_π, rather than σ, symmetry, and the negligible δ_π overlap affords a much longer Ru–Ru separation. The 35 kJ mol^{-1} separation between the minima in the $^2A_2''$ and $^2E''$ states reflects a strong electronic preference for the formation of a σ hemibonded structure.

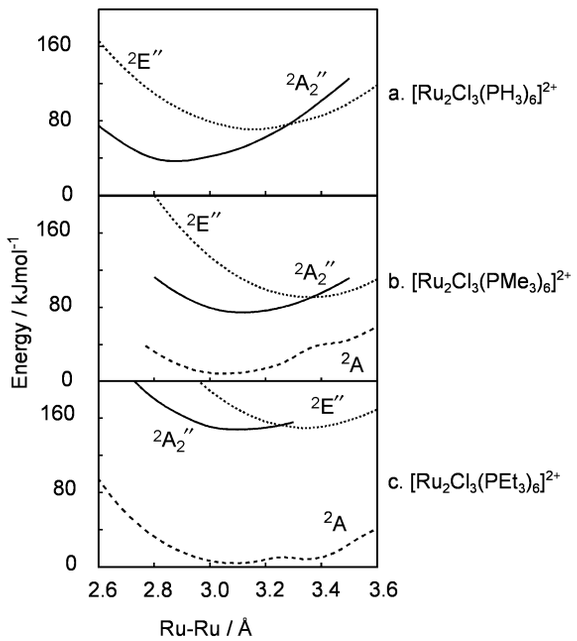

Fig. 2 Potential energy curves for non-symmetrised (^2A) and symmetrised ($^2A_2''$ and $^2E''$) states of $[Ru_2(\mu\text{-}Cl)_3(PR_3)_6]^{2+}$.

The introduction of methyl groups in their crystallographic (non-symmetrised) orientation breaks the three-fold symmetry, as a result of which both $^2A_2''$ and $^2E''$ states correlate with a single ^2A state in the C_1 point group. However, the potential energy curve for the ^2A ground state (Fig. 2b) exhibits very similar features to those in Fig. 2a, except that an avoided crossing permits a smooth transition from the σ-hemibonded state at short separations to its δ_π analogue at longer separations. As for the PH_3-capped species, the global minimum corresponds to the σ-hemibonded species, and, as was the case for the monocations, the methyl substituents cause only a marginal increase in the optimised Ru–Ru separation. Symmetrisation of the PMe_3 groups again increases the energy by approximately 50 kJ mol^{-1}, but, as was illustrated in the previous section, this is almost entirely due to interactions between the Me groups which are not of primary importance in the context of metal–metal interactions. The advantage of symmetrisation becomes clear at this point, as it allows us to locate separate minima for the $^2A_2''$ and $^2E''$ states, also shown in Fig. 2b. The optimised Ru–Ru separation of 3.05 Å in the $^2A_2''$ state is somewhat longer than in its non-symmetrised ^2A counterpart, due to increased repulsions with the bridge caused by the non-optimal orientation of substituents. Nevertheless, it is clear that the symmetrised and non-symmetrised structures afford an essentially convergent picture of the bonding. Significantly, the energetic separation between the $^2A_2''$ and $^2E''$ states is reduced from 35 kJ mol^{-1} in the PH_3-capped species to only 17 kJ mol^{-1} for the PMe_3 analogue, suggesting that the methyl groups destabilise the more weakly bonded $^2E''$ state to a lesser extent than $^2A_2''$. Further increasing the bulk of the substituent (PEt_3, Fig. 2c) induces changes that are entirely consistent with the previous discussion. With the non-symmetric crystallographic ligand orientation, the global minimum is found at Ru–Ru = 3.09 Å, although a second, higher lying local minimum emerges at approximately 3.35 Å. Symmetrisation of the ligand framework reveals $^2A_2''$ (Ru–Ru = 3.12 Å) and $^2E''$ (Ru–Ru = 3.33 Å) states that are separated by only 2 kJ mol^{-1}, and this near degeneracy leads to the emergence of the double minimum on the potential energy surface for the non-symmetrised species.

Table 5 Correlation between structural and spectroscopic parameters for (d^5d^6) species

	Ru–Ru[a]/Å	Calculated σ–σ* separation[a]/cm^{-1}	Observed σ–σ* energy/cm^{-1}
$[Ru_2(\mu\text{-}Cl)_3(NH_3)_6]^{2+}$	2.79	14160	17100 [16]
$[Ru_2(\mu\text{-}Cl)_3(PMe_3)_6]^{2+}$	3.05	8930	9350 [13]
$[Ru_2(\mu\text{-}Cl)_3(PEt_3)_6]^{2+}$	3.12	5460	7460 [13]

[a] In the $^2A_2''$ ground state in each case.

Thus, the rather different appearance of the potential energy curves for the non-symmetrised PH_3, PMe_3 and PEt_3 species can be traced to a relative destabilisation of the $^2A_2''$ state, where direct Ru–Ru σ bonding is present. The greater sensitivity of the $^2A_2''$ state to steric effects can, in turn, be traced to the non-bonded interactions between the substituents and the bridging halides, which, as noted above, naturally lead to an elongation of the Ru–Ru separation. As the Ru–Ru bond becomes stronger, and therefore shorter, the concertina motion of the Ru(μ-Cl)$_3$Ru unit will force the bridging halide groups into closer contact with the phosphine substituents, thereby magnifying the steric repulsions. The $^2A_2''$ state, where the Ru–Ru bond is shortest, is therefore inherently more sensitive to the steric bulk of the ligands than $^2E''$, and the effects of metal–metal bonding and steric repulsion are therefore in direct competition.

Implications for the spectra of the mixed-valence species

As noted in the introduction, Yeomans *et al.* have reported UV/visible spectra of mixed-valence $[Ru_2(\mu\text{-}Cl)_3(PR_3)_6]^{2+}$, R = Me and Et.[13] The positions of the σ⟶σ* transitions in these two complexes are collected in Table 5, along with the corresponding transition for the analogous ammine 'blue' $[Ru_2(\mu\text{-}Cl)_3(NH_3)_6]^{2+}$. Optimised Ru–Ru separations are also summarised ($^2A_2''$ ground state), along with the calculated separation of the σ and σ* orbitals at the optimised geometry (this has previously been shown to give a reliable estimate of the observed transition energy).[13] Crucially, the calculated Ru–Ru bond lengths and σ–σ* separations show a strong correlation with the observed spectroscopic transitions, suggesting that the QM/MM calculations are modelling the critical features of the system. It is important to emphasise that the properties of the system are determined by the nature of the $^2A_2''$ ground state. Thus, despite the presence of an additional low-lying local minimum in the potential energy curve, the PEt_3 system appears very similar to its PMe_3 analogue. The proximity of the $^2E''$ state, however, is an indication that the bulky ethyl groups are almost large enough to cause a complete switch in the nature of the ground state. In the next section, we show that just such a transition does occur for the trications.

Structure and bonding in $[Ru_2(\mu\text{-}Cl)_3(PR_3)_6]^{3+}$

For the trication, $[Ru_2(\mu\text{-}Cl)_3(PR_3)_6]^{3+}$, the removal of two electrons from the t_{2g} manifold gives rise to three distinct states in D_{3h} symmetry, depending on the location of the vacancies. Removal of two electrons from a non-degenerate orbital of a_2'' symmetry gives rise to a $^1A_1'$ state. In contrast, removal of two electrons from a degenerate e″ orbital gives rise to a $^3A_2'$ state (as well as excited $^1E'$ and $^1A_1'$), while removal of one electron from each orbital gives yields a $^3E'$ state. Potential energy curves for all three states of the parent complex $[Ru_2(\mu\text{-}Cl)_3(PH_3)_6]^{3+}$ are shown in Fig. 3a and optimised Ru–Ru separations and relative energies are summarised in Table 6. The global minimum is clearly the $^1A_1'$ state, with a short Ru–Ru separation of 2.71 Å, very similar to that in $[Ru_2(\mu\text{-}Cl)_3Cl_6]^{3-}$, and consistent with the presence of a covalent Ru–Ru σ bond. The $^3A_2'$ state, where any Ru–Ru bonding is necessarily localised within the weakly overlapping δ_π orbitals, lies some 50 kJ mol^{-1} higher in energy, and the optimised Ru–Ru separation of 3.21 Å confirms the absence of any significant interaction between the two metal centres. The $^3E'$ state with a single vacancy in the σ manifold, is intermediate between $^1A_1'$ and $^3A_2'$, both in energetic and structural terms.

Table 6 QM/MM optimised structural parameters for symmetrised states of $[Ru_2(\mu\text{-}Cl)_3(PR_3)_6]^{3+}$

		Ru–Ru/Å	E_{rel}/kJ mol^{-1}
$[Ru_2(\mu\text{-}Cl)_3(PH_3)_6]^{3+}$	$^1A_1'$	2.71	0
	$^3E'$	2.92	20
	$^3A_2'$	3.21	50
$[Ru_2(\mu\text{-}Cl)_3(PMe_3)_6]^{3+}$	$^1A_1'$	2.80	0
	$^3E'$	3.07	0.1
	$^3A_2'$	3.27	13
$[Ru_2(\mu\text{-}Cl)_3(PEt_3)_6]^{3+}$	$^1A_1'$	2.85	0
	$^3E'$	3.15	−16
	$^3A_2'$	3.35	−17

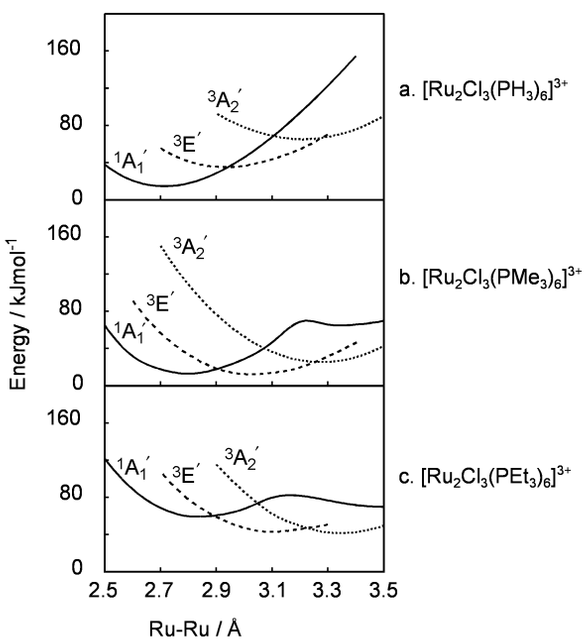

Fig. 3 Potential energy curves for symmetrised $^1A_1'$ and $^3E'$ and $^3A_2'$ states of $[Ru_2(\mu\text{-}Cl)_3(PR_3)_6]^{3+}$.

The introduction of methyl substituents in their crystallographically determined orientations again removes the symmetry-based distinction between the three states. The presence of two vacancies in the t_{2g} manifold results in considerable SCF convergence problems, and so the full non-symmetrised potential energy curve is not reported. Nevertheless, a minimum for $[Ru_2(\mu\text{-}Cl)_3(PMe_3)_6]^{3+}$ has been located (Table 6) with a Ru–Ru separation of 2.76 Å, similar to that in the $^1A_1'$ ground state of the parent phosphine, and the 0.05 Å increase in Ru–Ru distance is typical of the changes induced by the methyl groups in other oxidation states. Symmetrisation of the $(PMe_3)_3$ units allows us to recover the symmetry-based distinction between the three states, and confirms the $^1A_1'$ state as the most stable of the three, Fig. 3b. As might be anticipated on the basis of previous sections, the symmetrised $^1A_1'$ state lies approximately 50 kJ mol^{-1} above the non-symmetrised ground state and has a marginally longer Ru–Ru bond (2.80 Å). Thus we conclude that the ground state of $[Ru_2(\mu\text{-}Cl)_3(PMe_3)_6]^{3+}$ is remarkably similar

to its PH_3-capped parent, with a strong covalent Ru–Ru σ bond. A closer examination of the relative energies of the three states, $^1A_1'$, $^3E'$ and $^3A_2'$ does, however, reveal significant differences between the PH_3 and PMe_3-capped species. The fact that non-bonded repulsions between the bridging halides and the phosphine ligands are increased as the $\{Ru(\mu\text{-}Cl)_3Ru\}$ core is compressed has already been noted, and thus the influence of the methyl substituents should increase in the order $^3A_2' < {}^3E' < {}^1A_1'$. The relative energies of the three states confirm this expectation: whilst the $^1A_1'$ state was 20 kJ mol^{-1} more stable than $^3E'$ for the PH_3-capped species, the corresponding difference is only 0.1 kJ mol^{-1} for PMe_3. The separation between the $^3E'$ and $^3A_2'$ states is affected in a similar fashion, a gap of 30 kJ mol^{-1} for PH_3 being reduced to only 13 kJ mol^{-1} for PMe_3. The ethyl substituents further increase the non-bonded interactions with the bridge, leading to additional steric destabilisation, again in the order $^1A_1' > {}^3E' > {}^3A_2'$ (Fig. 3c). Critically, the steric effects are now so large that they cause a reversal in the energetic ordering of the three states, the most stable now being $^3A_2'$ (Ru–Ru = 3.35 Å) rather than $^1A_1'$, as was the case for PH_3- and PMe_3-capped species. Accordingly, the global ground state of the non-symmetrised complex is a triplet state (^3A) rather than a singlet, with a Ru–Ru separation of 3.34 Å, almost 0.5 Å longer than in the corresponding complex with PMe_3 ligands.

Summary

In this paper, we have examined the competition between covalent metal–metal bonding and steric repulsion in a series of closely related bimetallic species. The ability of steric effects to strongly perturb, and even eliminate, relatively weak bonds (notably agostic interactions) is well established, but for them to have a major impact on a covalent bond is rather more unexpected. The systematic variation of the metal–metal bond order from 0 to 1.0 in the redox-related ruthenium dimers described here provides an ideal opportunity to examine the interplay of these two factors. Somewhat surprisingly, steric effects are found to have the greatest influence where the Ru–Ru bond order is highest. Through an analysis of the relative energies of the various electronic states of the symmetrised molecules, we have shown that this apparently counterintuitive observation is a direct result of the nature of the steric interactions. These occur primarily between the substituents on the phosphines and the bridging halides, and, because enhanced metal–metal bonding displaces the bridging halides towards the alkyl substituents, states with short Ru–Ru bonds are necessarily the most sensitive to steric bulk. In the (d^5d^6) systems (2+), all three species (PH_3, PMe_3 and PEt_3-capped) share a common σ-hemibonded ground state ($^2A_2''$), and changing the phosphine induces only relatively minor changes in the Ru–Ru bond length. In contrast, at the (d^5d^5) level the bulky ethyl groups destabilise the σ bond to such an extent that the preferred ground state of $[Ru_2(\mu\text{-}Cl)_3(PEt_3)_6]^{3+}$ is in fact a triplet, with minimal direct Ru–Ru bonding. This complete switch in ground state is reflected in a dramatic (0.5 Å) increase in the Ru–Ru separation. The ability to modify and even eliminate covalent bonds by varying the steric bulk of remote substituents may provide a viable mechanism for tuning the properties of polymeric metal species.

Acknowledgements

The Engineering and Physical Sciences Research Council (UK) are gratefully acknowledged for financial support. S. Z. K. also acknowledges an ORS award.

References

1 For a review of recent applications of DFT to transition metal chemistry, see E. R. Davidson, *Chem. Rev.*, 2000, **100**, 351 and references therein.
2 (*a*) F. Maseras, *Chem. Commun.*, 2000, **19**, 1821–1827; (*b*) T. K. Woo, L. Cavallo and T. Ziegler, *Theor. Chem. Acc.*, 1998, **100**, 307–313.
3 (*a*) J. Jaffart, M. Etienne, F. Maseras, J. E. McGrady and O. Eisenstein, *J. Am. Chem. Soc.*, 2001, **123**, 6000–6013; (*b*) A. C. Cooper, E. Clot, J. C. Huffman, W. E. Streib, F. Maseras, O. Eisenstein and K. G. Caulton, *J. Am. Chem. Soc.*, 1999, **121**, 97–106.
4 (*a*) T. Lovell, R. Stranger, J. E. McGrady and S. A. Macgregor, *Inorg. Chem.*, 1996, **35**, 3079–3080; (*b*) J. E. McGrady, R. Stranger and T. Lovell, *Inorg. Chem.*, 1997, **36**, 3242–3247; (*c*) J. E. McGrady, R. Stranger and T. Lovell, *J. Phys. Chem. A*, 1997, **101**, 6265–6272; (*d*) T. Lovell, R. Stranger and J. E. McGrady, *Inorg. Chem.*, 2001, **40**, 39–43.
5 (*a*) J. E. McGrady, *J. Chem. Soc., Dalton Trans.*, 1999, 1393–1399; (*b*) J. E. McGrady, *Angew. Chem., Int. Ed.*, 2000, **39**, 3077–3079.
6 (*a*) U. Kölle, J. Kossakowski, N. Klaff, L. Wesemann, U. Englert and G. E. Heberich, *Angew. Chem.*, 1991, **103**, 732–733; U. Kölle, J. Kossakowski, N. Klaff, L. Wesemann, U. Englert and G. E. Heberich, *Angew. Chem., Int. Ed. Engl.*, 1991, **30**, 690–691; (*b*) U. Kölle, H. Lueken, K. Handrick, K. Schilder, J. K. Burdett and S. Balleza, *Inorg. Chem.*, 1995, **34**, 6273–6278.
7 R. Stranger, I. E. Grey, I. C. Madsen and P. W. Smith, *J. Solid State Chem.*, 1987, **69**, 162–170.
8 (*a*) G. A. Heath, D. C. R. Hockless and B. D. Yeomans, *Acta Crystallogr., Sect. C*, 1996, **52**, 854–858; (*b*) J. A. Statler, G. Wilkinson, M. Thornton-Pett and M. B. Hursthouse, *J. Chem. Soc., Dalton Trans.*, 1984, 1731–1738.
9 M. Laing and L. Pope, *Acta Crystallogr., Sect. B*, 1976, **32**, 1547–1550.
10 K. A. Raspin, *J. Chem. Soc. A*, 1969, 461–473.
11 F. A. Cotton and R. C. Torralba, *Inorg. Chem.*, 1991, **30**, 2196–2207.
12 L. F. Rhodes, C. Sorato, L. M. Venanzi and F. Bachechi, *Inorg. Chem.*, 1988, **27**, 604–610.
13 B. D. Yeomans, D. G. Humphrey and G. A. Heath, *J. Chem. Soc., Dalton Trans.*, 1997, 4153–4166.
14 M. N. Hughes, D. O'Reardon, R. K. Poole, M. Thornton-Pett and M. B. Hursthouse, *Polyhedron*, 1987, **6**, 1711–1713.
15 J. Darriet, *Rev. Chim. Miner.*, 1981, **18**, 27–32.
16 W. A. Clucas, R. S. Armstrong, I. E. Buys, T. W. Hambley and K. W. Nugent, *Inorg. Chem.*, 1996, **35**, 6789–6794.
17 ADF2002.02, Theoretical Chemistry, Vrije Universiteit, Amsterdam. (*a*) E. J. Baerends, D. E. Ellis and P. Ros, *Chem. Phys.*, 1973, **2**, 42–51; (*b*) G. te Velde and E. J. Baerends, *J. Comput. Phys.*, 1992, **99**, 84–98.
18 R. G. Parr and W. Yang, *Density Functional Theory of Atoms and Molecules*, Oxford University Press, New York, 1989.
19 S. H. Vosko, L. Wilk and M. Nusair, *Can. J. Phys.*, 1980, **58**, 1200–1211.
20 A. D. Becke, *Phys. Rev. A*, 1988, **38**, 3098–3100.
21 J. P. Perdew, *Phys. Rev. B*, 1986, **33**, 8822–8824.
22 L. Versluis and T. Ziegler, *J. Chem. Phys.*, 1988, **88**, 322–328.
23 M. Clark, R. D. Cramer III and N. Van Opdenbosch, *J. Comput. Chem.*, 1989, **10**, 982–1012.
24 A. K. Rappe, C. J. Casewit, K. S. Colwell, W. A. Goddard III and W. M. Skiff, *J. Am. Chem. Soc.*, 1992, **114**, 10024–10035.
25 P. E. Fanwick, I. F. Fraser, S. M. Tetrick and R. A. Walton, *Inorg. Chem.*, 1987, **26**, 3786–3791.